TOPICAL REVIEW • OPEN ACCESS

Acousto-optic systems for advanced microscopy

To cite this article: Martí Duocastella *et al* 2021 *J. Phys. Photonics* **3** 012004

View the article online for updates and enhancements.

Journal of Physics: Photonics

TOPICAL REVIEW

Acousto-optic systems for advanced microscopy

Martí Duocastella[1,2] , Salvatore Surdo[2], Alessandro Zunino[2,3], Alberto Diaspro[2,3] and Peter Saggau[2,4]

[1] Department of Applied Physics, Universitat de Barcelona, C/Martí i Franquès 1, 08028, Barcelona, Spain
[2] Nanoscopy, CHT Erzelli, Istituto Italiano di Tecnologia, Via Enrico Melen 83, Building B, 16152, Genova, Italy
[3] Department of Physics, University of Genoa, Via Dodecaneso 33, 16146, Genova, Italy
[4] Department of Neuroscience, Baylor College of Medicine, Houston, TX, United States of America

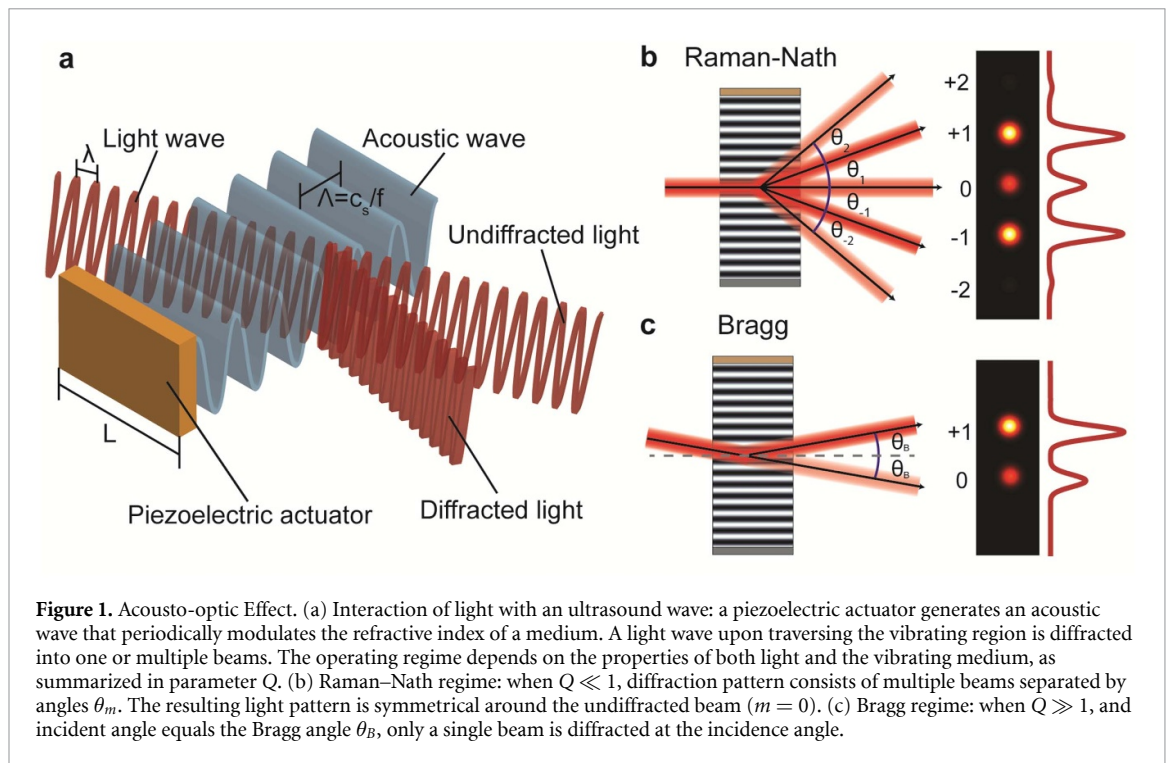E-mail: marti.duocastella@ub.edu and psaggau@bcm.edu

Abstract

Acoustic waves in an optical medium cause rapid periodic changes in the refraction index, leading to diffraction effects. Such acoustically controlled diffraction can be used to modulate, deflect, and focus light at microsecond timescales, paving the way for advanced optical microscopy designs that feature unprecedented spatiotemporal resolution. In this article, we review the operational principles, optical properties, and recent applications of acousto-optic (AO) systems for advanced microscopy, including random-access scanning, ultrafast confocal and multiphoton imaging, and fast inertia-free light-sheet microscopy. As AO technology is reaching maturity, designing new microscope architectures that utilize AO elements is more attractive than ever, providing new exciting opportunities in fields as impactful as optical metrology, neuroscience, embryogenesis, and high-content screening.

1. Introduction

Cornerstones in developing new optical technologies are systems capable of directly controlling light. Efforts in this direction have led to transformative advances in both research and industry, ranging from optical fibers for communication [1] to complex optical traps for laser cooling [2]. Among these technologies, advanced optical microscopy showcases the success of developing innovative strategies for guiding, focusing, splitting, and modulating light. Here, the optimal control of light directly determines the amount of information that can be retrieved from a sample. As such, modern microscopy architectures have come hand in hand with novel methods to increase speed, precision, and resolution at which light can be focused onto and collected from a sample. For instance, laser-scanning microscopes such as confocal [3] or multiphoton [4] systems—presently the tool-of-choice for cellular and functional tissue imaging—have flourished thanks to methods for precisely and swiftly scanning a focused laser beam across a sample. Similarly, the growing interest of light-sheet and structured-illumination microscopes (SIMs) [5] in the life sciences is mostly due to new approaches for shaping light beams [6, 7]. All in all, improvements in light control have radically changed optical microscopes, rendering them quantitative tools for characterizing living specimen with unprecedented spatial and temporal detail.

Several approaches exist to control illumination and detection of light in optical microscopes. They can be broadly divided into two groups: passive and active systems. The first group includes lenses, beam splitters, and diffractive optical elements, producing a static output for a given light input. While quality and customization has improved thanks to modern fabrication technologies such as three-dimensional (3D) printing of optical components [8, 9], their operational principle and implementation have remained largely unchanged. The second group, active systems, is capable of dynamically shaping light, and has seen a tremendous progress over the last decades. Examples include, spatial light modulators for multi-point illumination [10] and adaptive optics for reduction of aberrations [11], resonant scanning mirrors for reduced photobleaching [12], varifocal systems for fast axial focusing [13], and electro-optical scanners for fast imaging [14] and 3D particle tracking [15]. Among active systems, the family of acousto-optic (AO) devices stands out because of its versatility. AO devices enable high-speed modulation, deflection, splitting,

Figure 1. Acousto-optic Effect. (a) Interaction of light with an ultrasound wave: a piezoelectric actuator generates an acoustic wave that periodically modulates the refractive index of a medium. A light wave upon traversing the vibrating region is diffracted into one or multiple beams. The operating regime depends on the properties of both light and the vibrating medium, as summarized in parameter Q. (b) Raman–Nath regime: when $Q \ll 1$, diffraction pattern consists of multiple beams separated by angles θ_m. The resulting light pattern is symmetrical around the undiffracted beam ($m = 0$). (c) Bragg regime: when $Q \gg 1$, and incident angle equals the Bragg angle θ_B, only a single beam is diffracted at the incidence angle.

filtering, and focusing of light. These features, combined with their ease of implementation, have rendered them essential components of advanced optical microscopes.

In this review, we provide a comprehensive introduction to AO systems and their applications to optical microscopy. First, we describe the operation principles and properties of various AO devices, emphasizing the differences between members of the AO family and their early use in optical microscopes. Next, we survey recent developments in advanced microscopy that feature AO devices as enabling elements, including random-access scanning microscopes and fast volumetric imaging systems. They provide clear examples of the numerous possibilities that AO systems offer in imaging applications. Finally, we discuss how AO devices can help to continue shaping the present and future of optical microscopy.

2. How acousto-optic systems work

The large family of AO devices provides a complete toolkit for controlling light in microscopy applications, ranging from splitting to focusing beams as well as amplitude and frequency modulation. Despite the significant differences between AO devices, they all operate under the same physical principle, the so-called AO effect. This phenomenon consists of the diffraction of light by ultrasound waves [16]. Briefly, ultrasound is used to create regions of compression and rarefaction in an optical medium, which in turn, produce local changes in the refractive index (figure 1(a)). For typical AO materials (crystals and liquids) and ultrasound intensities, the maximum change in refractive index (Δn) ranges from 10^{-4} to 10^{-5}. When a beam of light propagates through such an acoustically perturbed medium, it undergoes a phase transformation, resulting in singular diffraction effects.

Depending on the properties of the vibrating medium (static refractive index n_0, thickness L, speed of sound c_s), the wavelength of light (λ), and the frequency of ultrasound (f), two different regimes can be identified leading to distinct diffraction patterns. While no sharp transition exists between them, it has proved useful to identify the two regimes by the parameter Q [17], defined as:

$$Q = \frac{2\pi \lambda L f^2}{n_0 c_s^{\,2}} \qquad (1)$$

The parameter Q quantifies the effective thickness of the vibrating medium. Depending on the magnitude of Q, two distinct diffraction phenomena are possible. When $Q \ll 1$, known as the *Raman–Nath regime*, the diffraction pattern consists of a fan of beamlets symmetrically spread with respect to the undiffracted beam (zero order). As shown in figure 1(b), each beamlet is diffracted at a fixed angle $\theta_m = m\lambda f / n_0 c_s$, and experiences a frequency shift mf, where m is an integer denoting the diffraction order. Thus, an AO device operated in this regime acts as a moving thin phase grating [18]. Although the splitting of

light into multiple beams forming an optical frequency comb is of great interest in microscopy, it comes with a caveat. The intensity of each beamlet is different, rapidly decaying for higher orders, and never reaching more than the 34% of the incident intensity. However, as detailed in the next sections, new AO devices used in microscopy for fast axial focus control or generating interference patterns do operate in this regime.

When $Q \gg 1$, known as the *Bragg regime*, the diffraction pattern typically contains a single diffraction order. For this to occur, the incident beam needs to enter the AO device at a particular angle, called the Bragg angle θ_B, given by the expression:

$$\sin\theta_B = \lambda f / 2n_0 c_s \qquad (2)$$

As shown in figure 1(c), such a condition, known as phase- or momentum-matching, leads to the deflection of the diffracted beam by an angle equal to θ_B, with a frequency shift of the light wave of $\pm f$ depending on the sign of the incident angle. Hence, the *Bragg regime* is optically equivalent to a moving thick phase grating. Notably, the beam diffracted after the AO device maintains most of the incident intensity, with typical maximum values in the range of 60%–100%. Such a high diffraction efficiency facilitates the integration of AO devices in optical microscopes as add-on modules (no need to increase the illumination power). It also helps to design systems for controlling light in different directions by cascading multiple AO devices.

The previous description, although general, does not provide a complete picture of the AO effect. Additional aspects need to be considered when selecting or designing an AO device for microscopy. Among them, the type of ultrasound waves—longitudinal or transverse and traveling or standing—is essential. In general, AO devices make use of longitudinal waves. However, transverse waves are preferred in specific applications such as beam deflection at high spatial resolution. Traveling waves are prevailing in most AO devices, particularly in those operating at the *Bragg regime*. In this case, besides the ultrasound generator, the AO device needs to incorporate an acoustic absorber at the opposite side to prevent unwanted sound reflections that may reduce the intensity of the diffracted beam. The main advantage of traveling waves is a continuous operating frequency band. Alternatively, standing waves are generally used with Raman–Nath diffraction. Because a resonant cavity is needed here that may be susceptible to temperature fluctuations, feedback systems are required to maintain the diffraction pattern at the discrete resonant conditions. Note, though, that diffraction generated by standing waves depends on time. Therefore, once steady-state is reached, it is possible to select different light patterns at high speed—only limited by the driving frequency [19]. Resonance also allows for minimal driving power of the ultrasound actuators.

The optical anisotropy of the medium also plays a pivotal role in AO devices, with direct consequences for microscopy applications. By using birefringent materials, the incident and diffracted angles are no longer the same. Thus, the range of incident beam angles, or the operative frequency bandwidth of AO devices can be significantly increased [20]. As detailed in the following section, most AO deflectors and all AO tunable filters use birefringent materials. Particularly, uniaxial crystals, exhibiting a crystal axis with a refractive index different from the other two. As a result of the anisotropy of these materials, careful attention must be paid to the polarization direction of both incident and diffracted beams relative to the orientation of the AO device. Thus, additional optical elements, such as adjustable waveplates, are normally required to successfully integrate AO devices into microscopes.
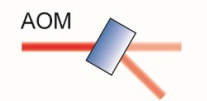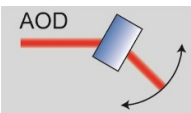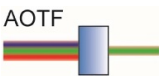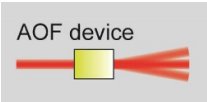
2.1. Types of acousto-optic devices

The need for optimizing the many facets of light control has spurred the development of an entire family of AO devices. They all operate under the same principle and also feature the same key elements, including an AO medium transparent to light, an ultrasound source (normally a piezoelectric transducer), and the control electronics. The latter enables adjusting frequency and amplitude of the driving signal, and consequently, the ultrasound waves and the diffraction regime. Because all AO devices achieve light control without the inertia of moving mechanical components, they have typical response times well below milliseconds. Despite these similarities, each AO device has distinct characteristics suitable for performing a specific task, as briefly summarized in table 1. Understanding these characteristics is vital for microscopy applications, where strict requirements exist regarding focusing precision and photon collection efficiency [21]. Next, we detail the main features of a selected number of AO devices that are relevant for advanced microscopy.

2.1.1. AO modulators

One of the most widely used AO devices in microscopy is the acousto-optic modulator (AOM). It is a common component in laser-scanning microscopes, including confocal or two-photon systems, for elegant electronic control of the illumination intensity. It is also used for generating a synchronization signal and for laser pulse picking. In all these applications, the AOM acts as a high-speed light attenuator.

Table 1. Types of acousto-optic devices. Top to bottom: acousto-optic modulator (AOM), acousto-optic deflector (AOD), acousto-optic tunable filter (AOTF), acousto-opto-fluidic (AOF) device, and tunable acoustic gradient (TAG) lens.

Device	Regime	Function	Main features	Cautionary remarks
AOM	Bragg	Optical attenuator	Contrast Rise time: 5–500 ns	Speed/efficiency trade-off
AOD	Bragg	Angular scanner	Angular range: 1–50 mrad Resolution: 5–500 spots	Speed/resolution trade-off
AOTF	Bragg	Wavelength selector	Bandwidth: 0.1–50 nm Tuning time: 1–10 μs	Efficiency up to 90%
AOF device	Raman–Nath	Pattern generator	Tunability Speed: 0.1–10 MHz	Diffracted beams are not independent
TAG lens	Raman–Nath	Varifocal lens	Optical power: 0–10 m^{-1} Speed: 0.01–1 MHz	Sinusoidal scanning

AOMs consist of a piezoelectric actuator bonded to a facet of a rectangular solid medium—typically a birefringent crystal or fused silica. As shown in table 1, AOMs are operated in the Bragg regime at a fixed driving frequency (40–200 MHz range), producing the splitting of an incident beam into two beamlets at a fixed angle. By tuning the sound amplitude, the relative intensity between the two beamlets can be modulated. Although both beamlets can be used for light modulation, the diffracted beam is usually preferred in microscopy. The latter grants high contrast between the minimum and maximum light intensity—from no light to about 70% of the incident light, given by the typical diffraction efficiency of AOMs. A central aspect of AOMs is their high-modulation speed, determined by the time to reach the maximum or minimum values of the diffracted light (rise and fall time). For a Gaussian beam of size w, the rise time is related to the acoustic *access time* τ, namely the time the ultrasound wave needs to traverse the light beam:

$$\tau \propto \mathrm{w}/c_s \tag{3}$$

Thus, an AOM typically features a small aperture, which requires it to be placed between two lenses, one for focusing and one for re-collimation of the beam. Using this strategy, the diffraction efficiency is reduced, but the benefit is a decrease in modulation time, down to tens of nanoseconds.

2.1.2. AO deflectors

Acousto-optic deflectors (AODs) are AO devices optimized to function as fast electronic beam scanners (see table 1). They are implemented in advanced laser-scanning systems to maximize the laser deflection speed, and consequently, the spatiotemporal resolution retrieved from dynamic samples [22]. They are also used to shift the frequency of the incident beam by a controlled amount. In this case, they are also known as acousto-optic frequency shifters (AOFS).

AODs share many resemblances with AOMs regarding design, geometry, and operational mode (*Bragg regime*). However, some singular and important differences exist. In AODs, beam scanning is obtained by tuning the driving frequency—the angle of the diffracted beam (Bragg angle) depends on this parameter (see equation (2)). Thus, an electronic driver capable of operation over a wide frequency range is needed. Blocking of the undiffracted beam is also required. Importantly, to maintain a high diffraction efficiency over a broad angular range $\Delta\theta_d$, AODs normally make use of birefringent materials. As previously described, for a fixed angle of incidence, the phase-matching condition only occurs at a given acoustic frequency. Birefringent materials, operated around the so-called tangential phase-matching, allow overcoming this issue and achieve an extended frequency band Δf, typically of 50 MHz or above.

In microscopy, maximizing Δf is not only crucial to achieve a high $\Delta\theta_d$, but also to increase the number of resolvable focal spots N, defined as:

$$N = \tau \Delta f \qquad (4)$$

where τ is the acoustic access time (see equation (3)). Notably, due to unavoidable beam divergence, resolution increases with beam diameter. Consequently, AODs commonly have an aperture much larger than AOMs. An aspect to consider is that both N and $\Delta\theta_d$ are larger for materials featuring a low speed of sound. Therefore, resolution and scanning range come at the cost of sacrificing speed: the response time of AODs is up to 4 orders of magnitude slower than AOMs, and within hundreds of microseconds. Still, AODs are amongst the fastest beam steering devices. It is also worth noting that the large acoustic bandwidth of AODs allows driving them with a multifrequency signal. In this case, each harmonic component diffracts the incident beam at its corresponding Bragg angle, resulting in an array of independently controlled beamlets.

2.1.3. AO tunable filters

Acousto-optic tunable filters (AOTFs) are AO devices that operate as electronically adjustable narrow-band-pass filters [23]. They are typically implemented in the beam-combining unit of laser-scanning systems to control intensity and wavelength of multiple laser lines. They can also be used as fast tunable beam splitters for multi-color imaging [24, 25].

AOTFs, similarly to AODS, also operate in the Bragg regime, exhibit a rectangular geometry, use birefringent crystals, and require electronic drivers with a wide frequency range. Indeed, by changing the driving frequency, the central wavelength λ_c of the passband that fulfills the phase-matching condition varies as:

$$\lambda_c = \frac{c_s \Delta n}{f} \qquad (5)$$

where Δn is the birefringence of the crystal. Critical parameters for selecting an AOTF in microscopy are the spectral resolution $\Delta\lambda$ and wavelength scan rate. Commercial AOTF can have a $\Delta\lambda$ as narrow as one nanometer or below. The scan rate, defined as the time needed to switch between beam wavelengths, depends on the acoustic access time, with typical values of a few microseconds.

A particular feature of AOTFs is the possibility to be implemented in the detection arm of a microscope for precise spectral imaging. Note, though, that the loss of light passing through the device, even if only 10%, is not ideal for fluorescence systems, in general having a low photon budget.

2.1.4. AOF device

Acousto-optofluidic devices (AOFs) function as electronic beam shapers to generate tunable optical patterns. They can be used for increasing imaging speed in laser-scanning systems or for producing light patterns in super-resolution techniques such as SIM.

In contrast to the AO devices previously described, AOFs consist of a liquid-filled chamber containing two pairs of orthogonally oriented piezoelectric actuators. Each actuator pair forms an acoustic resonant cavity. When driven on resonance, they produce ultrasound standing waves that diffract an incoming beam into an array of beamlets. Thus, the direct construction of 2D beam arrays is possible when both cavities are operative [26]. Interestingly, by adding a focusing lens between the device and the objective lens, the beamlets interfere, generating 3D patterns in the focal plane of the objective [19]. Note, although the latter is also possible with AODs, unavoidable crystal defects can deteriorate the pattern quality [27]. AOFs are operated at the *Raman–Nath regime*—as the significant acoustic attenuation of liquids at high frequencies makes it challenging to reach the Bragg regime. As such, AOFs offer a wide acceptance angle for the incident light, which eases alignment procedures and facilitates integration in microscopy systems.

The main features of AOFs are their high tunability and speed. By controlling the frequency and amplitude of the driving signal, the properties of the diffraction pattern, such as the number, spacing, and intensity of the diffraction orders, can be selected with the only constraint that the diffracted beams are not independent from each other. Also, the use of standing waves offers an extra control parameter. Employing synchronized pulsed illumination, the temporal phase difference between light pulses and the ultrasound wave enables to select a diffraction pattern faster than the acoustic access time. Given typical operation frequencies in the $0.5 - 5\,\mathrm{MHz}$ range, AOFs can operate at a timescale below $1\,\mu\mathrm{s}$.

2.1.5. TAG lens

Tunable acoustic gradient (TAG) lenses are AO devices operating as fast varifocal lenses. They are typically used in microscopy to extend the depth-of-field of high numerical aperture (NA) objective lenses, and as fast

axial scanners for high-speed volumetric imaging. Under certain conditions, they can also be used to generate Bessel beams [28–31].

TAG lenses have a cylindrical geometry, unique within the family of AO devices. They consist of a piezoelectric tube filled with a liquid. When driven on resonance, an ultrasound standing wave is formed, which can be described with a Bessel function [32]. Typically, a TAG lens requires the illumination beam clearly underfilling its aperture, in order to remain smaller than the central lobe of the Bessel function. In this mode, a TAG lens acts as a parabolic gradient-index lens, with the optical power $\delta(t)$ that periodically varies over time [29]:

$$\delta(t) = \frac{1}{F_{lens}(t)} = \frac{Ln_a\omega^2}{2c_s^2}\sin(\omega t) \qquad (6)$$

where F_{lens} is the focal length of the lens, L is the length of the tube, ω the angular driving frequency, and n_a is a constant that depends on ω and the liquid properties. The normal frequency range of a TAG lens is between 50 kHz and 1 MHz, and thus falls in the *Raman–Nath regime*. The effective NA of a TAG lens is low—as the aperture is limited by the central lobe of the Bessel function. Thus, for microscopy applications, TAG lenses are always used in combination with high NA objectives. By placing the TAG lens in a conjugate plane of the back focal plane of a microscope objective, magnification effects can be avoided, and the lens enables fast *z*-focus scanning. Such continuous *z*-focusing at microsecond time scales is faster than the integration time of many optical detectors. In this case, the simultaneous collection of multiple focal planes leads to an image with virtual extended depth-of-field. Notably, if synchronized stroboscopic illumination or fast detectors with appropriate electronics are used, information from multiple axial positions can be acquired.

When illuminated with a beam larger than the central lobe of the Bessel function, the TAG lens acts as an axicon with a user-selectable cone angle [32]. In this case, a Bessel-like beam is formed. Such a beam is of interest in microscopy, particularly in applications where fast interrogation of a volume without the need for axial resolution is required, as in some aspects of neuroimaging.

3. Recent applications of acousto-optic systems for advanced microscopy

The enormous advantages that AO devices offer regarding fast control of light have previously been utilized in microscopy. However, their use was limited to a small number of niche applications, such as laser power control (AOMs) and fast filters (AOTFs). With the advent of new technologies, including fast optical detectors, electronics, and digital acquisition cards, new opportunities for the use of AO devices in microscopy have emerged. Here we provide examples of how novel schemes, designed around AO devices, can help to enhance the performance of optical microscopes, allowing us to characterize relevant dynamic events at unprecedented spatiotemporal resolution.

3.1. Fast z-scanning volumetric microscopy
Maximizing the amount of spatial and temporal 3D-information retrieved from a sample is crucial in scientific and industrial applications ranging from cell imaging to optical inspection. Typically, 3D microscopes operate by acquiring a *z*-stack, namely a sequence of optical sections at different focal planes. Such a strategy requires techniques capable of optical sectioning, that is the virtual slicing of a sample into 2D sections [5]. In addition, the focus position must be axially translated. Unfortunately, fast *z*-focus scanning, a key factor in determining the overall volumetric imaging speed, has been technically challenging. Even today, most state-of-the-art 3D microscopes feature piezoelectric actuators for *z*-focusing via sample or objective lens translation. Due to inertia, the *z*-scanning rate is limited to a maximum of about 100 Hz. Thus, the *z*-axis has traditionally been the slowest scanning axis in a microscope system, imposing a burden when imaging fast dynamic processes. The implementation of AO systems, in particular the TAG lens, into 3D microscopes has helped to change this paradigm, effectively overcoming the restrictions in *z*-scanning speed.

3.1.1. Non-synchronized z-scanning
By conjugating the TAG lens to the back-aperture of a microscope objective lens, continuous *z*-focus scanning is attained at microsecond timescales. Such speed is faster than the exposure time or pixel dwell time of conventional microscope cameras. When using continuous illumination and/or non-synchronized detection, information from multiple focal planes is collected in a single-camera frame, obtaining an image with a dynamic extended depth-of-field [28]. The extent of the depth-of-field depends on the *z*-scanning range, which in turn is given by the driving voltage amplitude at the TAG lens and the NA and focal length of the objective lens. Typically, the depth-of-field can reach an extension of up to one order of magnitude relative to the native value of the focusing lens. Note, though, that the sinusoidal *z*-scanning produced by the TAG lens results in a non-uniform extended depth-of-field, with the scanned edges more intense than the
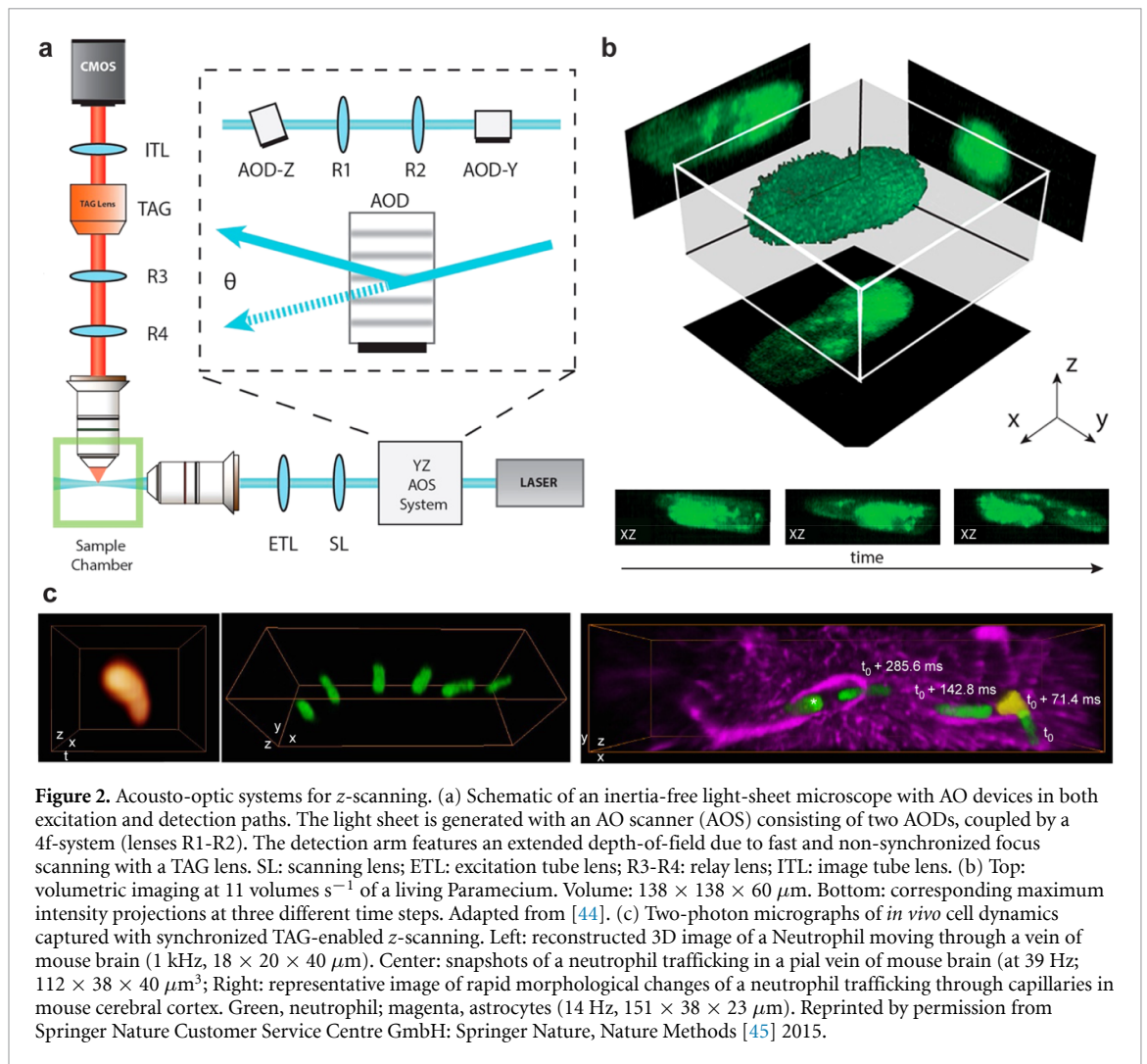
Figure 2. Acousto-optic systems for *z*-scanning. (a) Schematic of an inertia-free light-sheet microscope with AO devices in both excitation and detection paths. The light sheet is generated with an AO scanner (AOS) consisting of two AODs, coupled by a 4f-system (lenses R1-R2). The detection arm features an extended depth-of-field due to fast and non-synchronized focus scanning with a TAG lens. SL: scanning lens; ETL: excitation tube lens; R3-R4: relay lens; ITL: image tube lens. (b) Top: volumetric imaging at 11 volumes s^{-1} of a living Paramecium. Volume: $138 \times 138 \times 60$ μm. Bottom: corresponding maximum intensity projections at three different time steps. Adapted from [44]. (c) Two-photon micrographs of *in vivo* cell dynamics captured with synchronized TAG-enabled *z*-scanning. Left: reconstructed 3D image of a Neutrophil moving through a vein of mouse brain (1 kHz, $18 \times 20 \times 40$ μm). Center: snapshots of a neutrophil trafficking in a pial vein of mouse brain (at 39 Hz; $112 \times 38 \times 40$ μm^3; Right: representative image of rapid morphological changes of a neutrophil trafficking through capillaries in mouse cerebral cortex. Green, neutrophil; magenta, astrocytes (14 Hz, $151 \times 38 \times 23$ μm). Reprinted by permission from Springer Nature Customer Service Centre GmbH: Springer Nature, Nature Methods [45] 2015.

central part [33–35]. This effect is more pronounced as the scanned range increases, but it can be partially compensated by using synchronized illumination [36, 37] (see section 3.1.2). Also, the increase in spherical aberration as one moves away from the native focal plane of the objective lens, a usually detrimental effect when trying to maximize the extended depth-of-field, can help here to render the scanned volume uniform [13]. TAG lens-enabled bright-field microscopes, combined with edge detection methods or other image processing algorithms, have become valuable tools for 'extended depth-of-field' imaging in fast industrial metrology applications and quality-control tasks [38]. Additionally, the tunable depth-of-field of the TAG lens has been used in two-photon microscopy [28], optical coherence tomography [39] and photoacoustic microscopy [40] for rapid interrogation of volumes and enhanced image quality.

Interestingly, full 3D information from a sample can be retrieved in a light-sheet microscope featuring extended depth-of-field detection. In such microscopes, the sample is selectively illuminated with a thin sheet of light placed at the focal plane of an orthogonally oriented detection objective. Volumetric imaging is then performed by acquiring a *z*-stack where both illumination and detection objectives need to move synchronously. Given the slow speed of *z*-focus translation, such an operation can be time-consuming. Variable focal elements that provide remote *z*-focus control can relax these speed constraints [13, 41]. An even faster approach is to use an objective with an extended depth-of-field in the detection arm [42, 43]. Because an in-focus image is obtained for any plane at any position, the sole translation of the light-sheet suffices to collect the *z*-stack. In addition, volumetric imaging speed only depends on camera frame rate, light-sheet translation speed, and signal-to-noise ratio (SNR). As shown in figure 2(a), by using AOD scanning for translating the light sheet, a TAG lens for dynamic extended depth-of-field and a high-speed camera (10 000 frames s^{-1}), dark-field 3D images at sub-cellular resolution and rates as high as 200 volumes per second have been obtained. The same microscope has proven effective for fast *in vivo* imaging of biological systems (figure 2(b),c).

The acquisition rate can potentially be doubled by using two Gaussian beams and sweeping them across the field of view synchronously, using a CMOS camera with a double rolling shutter [46]. Despite the

high-speed capabilities of light-sheet microscopes with extended depth-of-field detection, extending the depth-of-field normally comes at the cost of losing signal. Parallelized illumination with multiple light sheets can significantly mitigate this effect [47].

3.1.2. Synchronized z-scanning

An alternative method for obtaining fast 3D images is to synchronize the TAG lens *z*-scanning with pulsed illumination[29, 30, 48–50]. Provided the pulse duration is shorter than the time it takes to hop from one plane to another (sub-microseconds), a particular *z*-position can be selected. The resulting imaging speed is no longer limited by *z*-focusing, but rather by the camera frame rate or, ultimately, the SNR. Note that such a strategy results in a significant reduction of SNR. Indeed, collecting light is limited to a fraction of the entire camera exposure or pixel dwell time. Still, current light sources, such as light-emitting diodes or certain lasers, are capable of pulsed operation, which makes synchronized strobing illumination easy to implement. This approach has been successfully used for fast micro-particle velocimetry inside microchannels [48] or optical inspection of consumer goods [38]. Importantly, the use of strobing light with an inter-pulse separation longer than the triplet state relaxation time of the fluorescent dyes, can have the added benefit of reducing photobleaching or phototoxicity [13, 51].

A fast 3D stack can also be collected by synchronizing the TAG lens with fast optical detection [45, 52]. By tagging the photons with their arrival time relative to the TAG lens position, a *z*-stack can be reconstructed in a post-processing step. Note that such operation requires detectors and data acquisition hardware with sub-microsecond response time. Thus, this strategy is more suitable for laser-scanning microscopes such as confocal or two-photon systems that feature point detectors. Similarly, fast electronics cards based on field programmable gate arrays are preferred for data acquisition [53]. Despite the added complexity regarding electronics, this approach offers two important advantages compared to synchronized illumination. First, valuable information can be collected during the entire pixel dwell time, resulting in improved SNR. Secondly, the number of sections of the *z*-stack can be arbitrarily selected during a post-processing step. As shown in figures 2(d)–(f), TAG lens-enabled microscopes with synchronized detection have been successfully implemented in several applications. They include fast fluorescence correlation spectroscopy [54], confocal microscopy [52], flow cytometry [55], or two-photon *in vitro* [31] and *in vivo* imaging [45, 53]. It is worth to note that the high-speed 3D light control offered by a laser-scanning microscope featuring a TAG lens can be used for operations beyond imaging, such as single-particle tracking [15], sample movements tracking [56, 57], or combined laser photo-stimulation with functional imaging [58].

3.2. Random-access scanning microscopy

Random-access microscopy or RAM is an imaging method implemented in laser-scanning microscopes and characterized by focusing a laser beam at a discrete number of individual and user-selectable sites of a specimen. The rationale of this approach is to drastically reduce acquisition time by interrogating a limited number of pre-selected points or regions of interest within the sample. As described in section 3.1, confocal or two-photon microscopes retrieve information from a volume by sequentially scanning an extensive collection of pixels, each requiring a particular illumination time (pixel dwell time). In sparse samples or when only specific parts of the sample are of interest, interrogating the entire volume is inefficient. RAM addresses this issue by restricting the collection of information to only selected regions of interest by using a two-step process. First, the regions of interest are selected. This task is performed by acquiring a conventional confocal or two-photon 3D image. Second, the laser focus is programmed to hop from one position to another. To minimize waiting time, light hopping should occur as fast as possible. High speed and accuracy of beam positioning have rendered AODs the tool-of-choice for implementing RAM.

3.2.1. 2D-RAM

As described in section 2.1, varying the driving frequency of AODs allows for scanning a laser beam along one direction (1D scan). Such scanning can be performed either continuously [59, 60], or at discrete positions [61, 62]. Since AODs do not use movable mechanical parts and are not limited by inertia, changing the deflection angle can be extremely fast, down to microsecond timescales [63]. Importantly, 1D scans can be extended to 2D scans by properly arranging two orthogonal AODs in series [61, 62]. In this scheme, each AOD controls the *x*- and *y*-axis deflections independently, enabling illumination of an arbitrary number of spots within a plane. The high versatility of 2D-AOD scanning has been exploited in optogenetics, where selective illumination of a sample is key. Examples include mapping the functional synaptic connections between neurons *in vitro* [64] and *in vivo* [65] as well as studying the role of GABA receptors in orthodromic propagation of axonal action potentials [66]. However, the central application of AODs has arguably been RAM.

The first RAM systems were implemented using 2D-AOD scanners and single-point detectors in a non-descanned configuration. While not capable of optical sectioning and featuring a relatively low spatial resolution, they enabled beam re-positioning in only 3–5 μs and acquisition rates as high as 200 ksamples s^{-1} [61]. Integration of 2D-AODs into confocal microscopes enabled a five-fold enhancement in the axial resolution while maintaining impressive frame rates, as high as 25 kHz [67]. Such a system, though, comes at the cost of increased complexity. Specifically, an array of pinholes is required in the detection arm. To this end, a digital micromirror device (DMD) can be used. Unfortunately, the effective pinhole size using a DMD is typically two-fold larger than in conventional confocal systems, resulting in reduced rejection of out-of-focus light .

Today, RAM is almost exclusively used with two-photon microscopes. In this case, tightly focused femtosecond laser pulses confine light emission to the focal volume [68], obviating the need for detection pinholes. Thus, the integration of 2D-AOD systems into two-photon microscopes comes at relative ease. Additionally, the core advantages of AO systems (speed, versatility) and two-photon microscopes (3D sub-cellular imaging at depth) are preserved. All these properties have rendered RAM particularly suitable for *in vivo* monitoring of dynamic events that are sparsely located. Given that such settings are typically found in neuroscience applications, particularly in functional brain imaging, it comes as no surprise that RAM has found its niche application in this field.
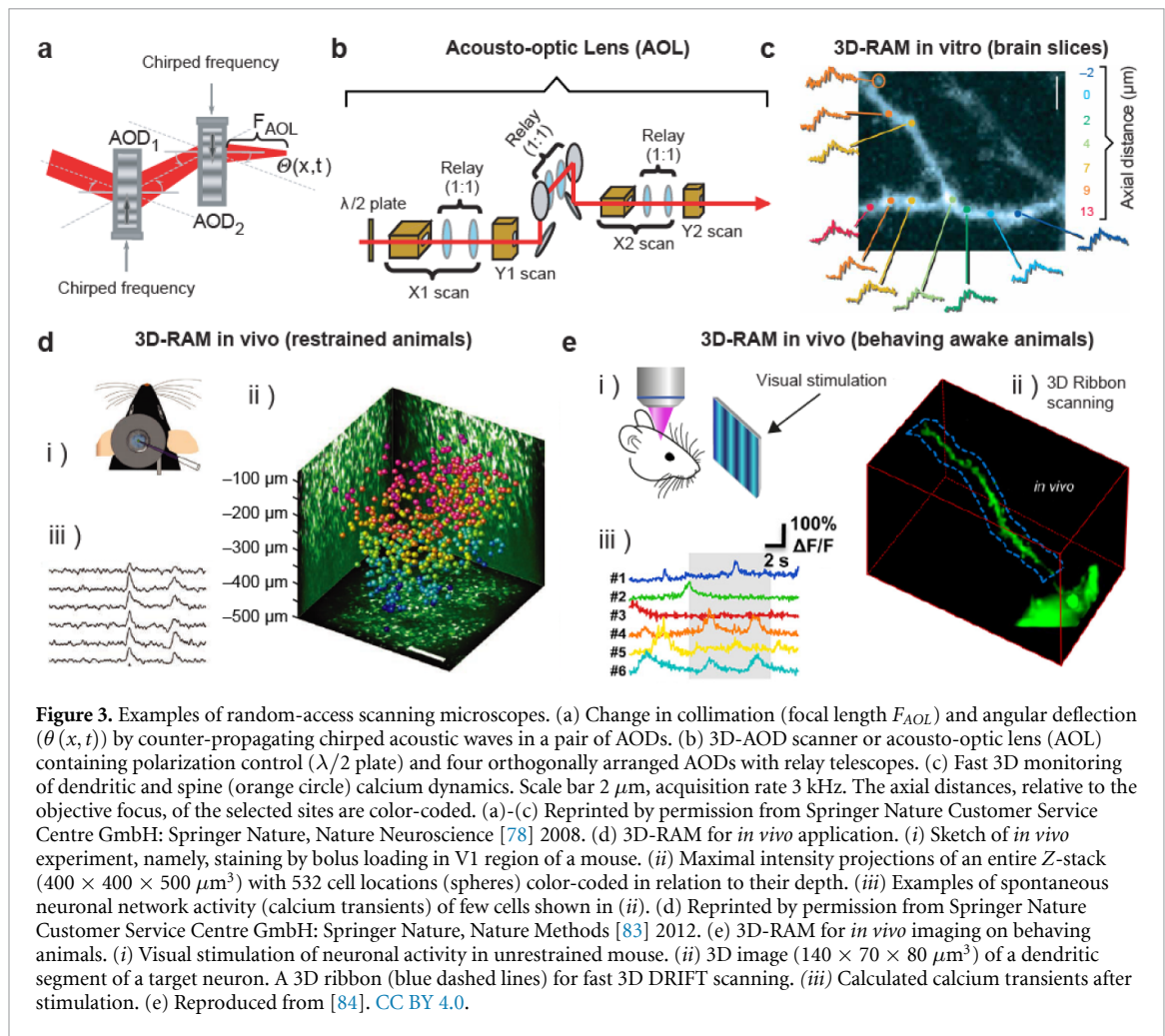
Even if two-photon systems are the prevailing RAM technology, they can face issues regarding the spatiotemporal dispersion of short laser pulses induced by the diffractive nature of AODs. Temporal dispersion broadens the pulse width, lowering the laser peak-power and, hence, the two-photon excitation efficiency. Spatial dispersion results in the spectral decomposition of the laser pulse, significantly reducing the number of resolvable spots of the AOD scanner. Both effects can be compensated, but careful attention is needed. In the case of temporal dispersion, pre-chirping of the laser pulse is the most common strategy. It is generally implemented with a pair of two identical prisms that introduce a negative dispersion depending on their separation. While an inter-prism separation of 65 cm has proven sufficient for compensating ∼90% of the dispersion introduced by the AODs [22], in some instances it may take distances as long as 4 meters— impracticable in many laboratories or commercial systems. Fortunately, more compact approaches such as stacked-prisms [69] or placing a tilted prism before the AODs offer viable alternatives [70–72]. Regarding spatial dispersion, the straightforward solution would be to use longer laser pulses (300–700 fs) which feature a narrower spectral bandwidth [73, 74]. Unfortunately, such pulse durations also results in lower two-photon signal, which can be detrimental in applications where excitation efficiency is low. In these cases, compression of the laser pulse by a diffraction grating [69, 75], an AOM [76], or a single prism [22] is possible. Interestingly, the latter two can be used to compensate for both spatial and temporal distortions.

RAM systems featuring 2D-AODs with well-compensated spatiotemporal distortions have been successfully used to characterize several key processes in the field of neurosciences. Examples include multisite uncaging of neurotransmitters at high spatial resolution (∼0.75 μm) [75], monitoring fast neural events such as synaptic or action potentials, rapid (frame rates 0.5–1.5 kHz) recording of calcium transients from several (up to 80) spines of the dendritic tree [73], identifying the direction of neural network activation with single-cell resolution in brain slices to study epilepsy [77], or obtaining fluorescence measurements from various neurons (up to 91) at a sampling rate of 180–490 Hz from layer L2/3 of mouse cortices *in vivo*.[11]

3.2.2. 3D-RAM

The RAM systems presented so far restricted fast scanning to a single 2D plane. Given the complex 3D organization of cellular structures such as the brain, extending fast scanning to a whole volume is a central aspect in RAM. While several variable optical elements exist for fast *z*-scanning [13], two pairs of 2D-AOD scanners operating in series can also be used for this purpose. As shown in figure 3(a), each pair of scanners must be driven by chirped and counter-propagating acoustic waves [62, 78, 79]. Such a combination results into two independent effects: (1) the beam is deflected in one direction with an angle proportional to the difference between the central frequencies of the AODs; (2) beam convergence or divergence is introduced because the AODs act as a cylindrical lens with a focal length inversely proportional the to the rate of change in frequency (chirp) [80]. Therefore, orthogonally cascading two scanners results in beam deflection in *x* and *y*, together with a 3D spherical change of the beam collimation. Optically conjugating the pair of 2D-AODs with a focusing lens enables fast *x, y, z* focus control (figure 3(b)). Note that, because four AODs are used in such a 3D-scanning system, only the effects of temporal dispersion must be taken into consideration. However, changing the collimation of the incident beam for *z*-scanning can result in spherical aberration [13]. This issue can be addressed by using synchronized illumination, in which case the AODs can act as beam shapers [81, 82].

Over the last decade, RAM utilizing 3D-AOD scanners has become an increasingly popular technique in neuroscience. As shown in figure 3(c), such systems have been used for monitoring 3D localized calcium

Figure 3. Examples of random-access scanning microscopes. (a) Change in collimation (focal length F_{AOL}) and angular deflection ($\theta(x,t)$) by counter-propagating chirped acoustic waves in a pair of AODs. (b) 3D-AOD scanner or acousto-optic lens (AOL) containing polarization control ($\lambda/2$ plate) and four orthogonally arranged AODs with relay telescopes. (c) Fast 3D monitoring of dendritic and spine (orange circle) calcium dynamics. Scale bar 2 μm, acquisition rate 3 kHz. The axial distances, relative to the objective focus, of the selected sites are color-coded. (a)-(c) Reprinted by permission from Springer Nature Customer Service Centre GmbH: Springer Nature, Nature Neuroscience [78] 2008. (d) 3D-RAM for *in vivo* application. (*i*) Sketch of *in vivo* experiment, namely, staining by bolus loading in V1 region of a mouse. (*ii*) Maximal intensity projections of an entire Z-stack ($400 \times 400 \times 500 \ \mu$m³) with 532 cell locations (spheres) color-coded in relation to their depth. (*iii*) Examples of spontaneous neuronal network activity (calcium transients) of few cells shown in (*ii*). (d) Reprinted by permission from Springer Nature Customer Service Centre GmbH: Springer Nature, Nature Methods [83] 2012. (e) 3D-RAM for *in vivo* imaging on behaving animals. (*i*) Visual stimulation of neuronal activity in unrestrained mouse. (*ii*) 3D image ($140 \times 70 \times 80 \ \mu$m³) of a dendritic segment of a target neuron. A 3D ribbon (blue dashed lines) for fast 3D DRIFT scanning. (*iii*) Calculated calcium transients after stimulation. (e) Reproduced from [84]. CC BY 4.0.
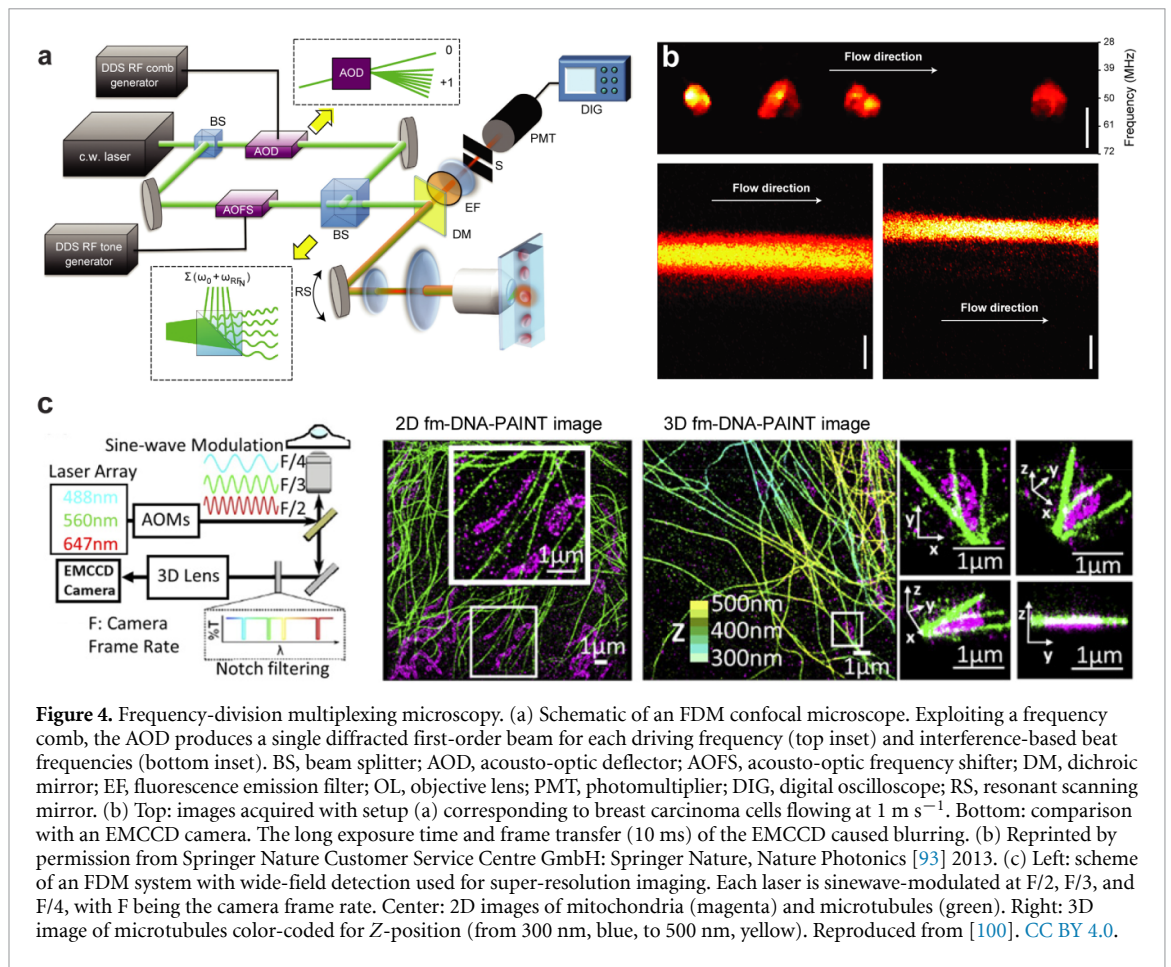
transients at rates as high as 10 kHz *in vitro* [78], as well as *in vivo* with synthetic [85] and long-wavelength genetically encoded indicators [86]. Note that, to maximize the scanned volume, wide-band AODs capable of wider deflections are required [87]. With such AODs, volumes as large as $700 \times 700 \times 1400 \ \mu$m³ were scanned at sub-millisecond speed and sub-cellular spatial resolution, enabling recording the calcium activity of more than 500 neurons [83].

An important aspect when applying 3D-RAM in awake behaving animals are motion artifacts, induced by heartbeat, respiration, as well as any muscle contraction [84, 88]. As this can change the location of tissue details relative to the pre-selected scanning sites, dynamic correction is necessary for long-term experiments. Such an effect can be corrected by a nonlinear (parabolic) chirp of the acoustic waves. Thus, pre-selected scanning points can be converted into small 3D lines, surfaces, and volumes (ribbons) that can used to compensate for possible focal shifts. As shown in figure 3(e), this strategy enabled measurements of neuronal activity on behaving animals, down to the spiny dendritic segments, over an axial range of 650 μm.

3.3. Frequency-division multiplexing microscopy

Besides fast z-scanning and hopping from one region to another within a sample, AO devices can be used to boost the 2D imaging speed. The straightforward application is to use AODs for rapid scanning in confocal or two-photon microscopes [89]. In these cases, though, even faster approaches exist such as the widely commercialized resonant galvo-scanners [90]. More recent applications have combined parallelization methods with AO devices. Examples include the use of beam-splitting gratings [91] and multiple illumination paths, each resulting in a different z-focus position [92]. Among them, frequency-division multiplexing (FDM) microscopy offers arguably the fastest 2D imaging speed.

The essence of FDM is to simultaneously illuminate multiple points of a sample, each at a specific temporal frequency. Thus, there is a univocal relationship between modulated frequency and position. In other words, the position is encoded in the frequency. The overall signal from the sample is recorded with a single photodetector. By decoding the signal in the frequency domain, e.g. using a Fourier transform, the intensity of each frequency component can be retrieved, and consequently, an image can be reconstructed.

Figure 4. Frequency-division multiplexing microscopy. (a) Schematic of an FDM confocal microscope. Exploiting a frequency comb, the AOD produces a single diffracted first-order beam for each driving frequency (top inset) and interference-based beat frequencies (bottom inset). BS, beam splitter; AOD, acousto-optic deflector; AOFS, acousto-optic frequency shifter; DM, dichroic mirror; EF, fluorescence emission filter; OL, objective lens; PMT, photomultiplier; DIG, digital oscilloscope; RS, resonant scanning mirror. (b) Top: images acquired with setup (a) corresponding to breast carcinoma cells flowing at 1 m s^{-1}. Bottom: comparison with an EMCCD camera. The long exposure time and frame transfer (10 ms) of the EMCCD caused blurring. (b) Reprinted by permission from Springer Nature Customer Service Centre GmbH: Springer Nature, Nature Photonics [93] 2013. (c) Left: scheme of an FDM system with wide-field detection used for super-resolution imaging. Each laser is sinewave-modulated at F/2, F/3, and F/4, with F being the camera frame rate. Center: 2D images of mitochondria (magenta) and microtubules (green). Right: 3D image of microtubules color-coded for Z-position (from 300 nm, blue, to 500 nm, yellow). Reproduced from [100]. CC BY 4.0.

As in FDM used in telecommunications, this strategy increases the rate of data recording by dividing the available detection band into multiple non-overlapping frequency channels, each carrying a separate signal. Compared to sequential scanning methods, and provided a frequency bandwidth large enough, FDM can increase the imaging speed by a factor equal to the number of illuminating points. Note, though, that this imaging modality typically needs relative long acquisition times to resolve the individual frequency components, depending on their period duration. Therefore, it is essential to modulate the excitation light at high frequencies. The ability of AO devices to frequency-shift the diffracted light renders them optimal tools for modulating light in the MHz-range. At such high-modulation frequencies, FDM enables imaging at rates at thousands of frames per second.

Given the intrinsic high speed of single-point photodetectors, FDM is most commonly implemented in laser-scanning systems [93–96]. As shown in figure 4(a), the typical elements consist of a single AOD and an AOFS. By driving the AOD with different radiofrequencies, a 1D comb of beamlets is obtained, each with a given deflection angle and frequency shift (tone). By interfering such multi-tone comb with the beam providing from the output of the AOFS (reference beam), the intensity of each beamlet can be modulated at MHz-range. Indeed, the interfering process results in frequency beats, whose frequency is the difference between the tone of each beamlet and that of the reference beam. When illuminating a fluorescent or scattering sample [97, 98] with such a comb of modulated beamlets, the univocal relationship between position and modulation frequency is established. Combining two AODs can result in 2D-combs of beamlets, enabling direct reconstruction of 2D images [99]. In most common implementations, though, the sample is illuminated with only 1D-line, thus requiring additional scanning for 2D or 3D images. While traditional galvo-scanners can be used [95], this extra degree of freedom is intrinsic to imaging flow cytometry systems. In this case, the temporal displacement of objects flowing in microfluidic channels acts as an additional scanned axis (see figure 4(b)). By using the 1D-comb of modulating beamlets to illuminate the direction perpendicular to the flow, 2D fluorescence confocal images have been acquired at kHz rates [93], with the main speed limited being imposed by the fluorescence lifetime of the fluorophore [94]. By combining flow imaging with z-focusing methods, z-stacks can be acquired. Using this strategy, 3D images of microalgal cells have been acquired at 100 volumes per second without motion blurring [94].

FDM can also be implemented in wide-field imaging systems, such as light-sheet [101] and super-resolution microscopes based on single molecule localization approaches [100]. These systems cannot

perform as fast as the previously described ones due to the limited frame rate of cameras. Still, they can outperform traditional implementations. For instance, by modulating different colors, each with a particular frequency, simultaneous super-resolution multi-color imaging using a monochromatic camera becomes possible (figures 4(c)–(e)). The gain in speed is proportional of the number of colors detected, while the localization precision of the native microscope is maintained.

Advantages of FDM, besides speed, are the possibility to improve the SNR of the reconstructed image. By applying lock-in detection algorithms, each unique beat frequency can be retrieved while filtering out any external source of noise. However, the shot-noise of each point (plane) is shared by all the multiplexed points (planes). This can be specially detrimental when imaging bright objects close to dim ones, however synthetically extending the acquisition time by phase-matching techniques can mitigate this effect [95]. Another advantage of the technique is the compatibility with highly scattering samples. Specifically, FDM combined with wavefront shaping has been successfully used to enhanced the laser focused intensity by a factor of 125 inside a 3 mm-thick chicken breast [99]. Special consideration must be given to the modulation bandwidth of AO devices and crosstalk between frequency beats. Typically, a large tone spacing is desirable to facilitate image reconstruction and avoid crosstalk. Unfortunately, the limited modulation bandwidth of AO devices determines the number of points that can be simultaneously illuminated. Strategies to increase such bandwidth include quadrature amplitude modulation [94]. Also, by properly selecting the phase of each tone or using machine-learning algorithms [102], crosstalk effects can be reduced. Today, state-of-the-art FDM systems feature about 100 comb lines with tone spacing of 1 MHz and a bandwidth of 200 MHz.

4. Summary and future outlook

The inertia-free nature and tunability of AO devices enables unprecedented light control in optical microscopy, opening the door to advancing research in important areas such as optical inspection, metrology or biology. Here we provided some key examples to illustrate how the unique properties of AO devices enable novel microscope designs capable of volumetric imaging at high spatiotemporal resolution. Thus, the fast z-scanning of a TAG lens allows rapid collection of a z-stack or dynamic extension of the depth-of-field of a microscope, significantly reducing 3D acquisition time. Similarly, selection and superimposition of the acoustic frequencies applied to an AOD has been recognized as the primary enabler of advanced scanning strategies in confocal and two-photon microscopes that further boost imaging rates by scanning pre-selected points of a volume or encoding spatial information in the frequency domain. As a result of these new developments, it is possible today to study fast dynamic processes such as neuronal communication at the cellular level and sub-millisecond resolution. The future of AO for optical microscopy looks even brighter. As progress will be made in the speed and sensitivity of light detectors [103, 104], volumetric imaging will be performed at even higher spatial resolution and speed. Combined with the help of artificial intelligence [105] or fast algorithms [106, 107], AO devices will increasingly become a fundamental tool of advanced imaging systems.

In order to keep this review compact, certain topics were not addressed here, including the use of AO devices for improving the spatial resolution of microscopes beyond the diffraction limit. In this regard, AOD systems have already been used in super-resolution systems based on single molecule localization [100], stimulated emission depletion microscopy [108], or SIM [27]. As new AO devices are being developed for dynamic light pattern generation, such as the recently implemented AOF [19], faster super-resolution methods with minimal photobleaching will become possible. Based on these results, we envision future AO systems that will continue to push the limits of optical microscopy, offering new opportunities to study biological processes at high spatiotemporal resolution and over a large volume, thus providing a clearer picture of living organisms and their functions from the molecular to the macroscopic scale.

Acknowledgments

ORCID iD

Martí Duocastella ● https://orcid.org/0000-0003-4687-8233

References

[1] Xavier G B and Lima G 2020 Quantum information processing with space-division multiplexing optical fibres *Commun. Phys.* **3** 1–11

[2] Seletskiy D V, Epstein R and Sheik-Bahae M 2016 Laser cooling in solids: advances and prospects *Rep. Prog. Phys.* **79** 096401

[3] Conchello J and Lichtman J W 2005 Optical sectioning microscopy *Nat. Methods* **2** 920–31

[4] Helmchen F and Denk W 2005 Deep tissue two-photon microscopy *Nat. Methods* **2** 932–40

[5] Mertz J 2011 Optical sectioning microscopy with planar or structured illumination *Nat. Methods* **8** 811–9

[6] Chang B J, Kittisopikul M, Dean K M, Roudot P, Welf E S and Fiolka R 2019 Universal light-sheet generation with field synthesis *Nat. Methods* **16** 235–8

[7] Chen B C *et al* 2014 Lattice light-sheet microscopy: imaging molecules to embryos at high spatiotemporal resolution *Science* **346** 1257998

[8] Gissibl T, Thiele S, Herkommer A and Giessen H 2016 Two-photon direct laser writing of ultracompact multi-lens objectives *Nat. Photon.* **10** 554–60

[9] Surdo S, Carzino R, Diaspro A and Duocastella M 2018 Single-shot laser additive manufacturing of high fill-factor microlens arrays *Adv. Opt. Mater.* **6** 1701190

[10] Nikolenko V, Watson B O, Araya R, Woodruff A, Peterka D S and Yuste R 2008 SLM microscopy: scanless two-photon imaging and photostimulation with spatial light modulators *Front. Neural Circuits* **2** 5

[11] Booth M J 2014 Adaptive optical microscopy: the ongoing quest for a perfect image *Light Sci. Appl.* **3** e165–e165

[12] Wu Y, Wu X, Lu R, Zhang J, Toro L and Stefani E 2015 Resonant scanning with large field of view reduces photobleaching and enhances fluorescence yield in STED microscopy *Sci. Rep.* **5** 14766

[13] Kang S K, Duocastella M and Arnold C B 2020 : Variable optical elements for fast focus control *Nat. Photon.* **14** 533-42

[14] Schneider J, Zahn J, Maglione M, Sigrist S J, Marquard J, Chojnacki J, Kräusslich H-G, Sahl S J, Engelhardt J and Hell S W 2015 Ultrafast, temporally stochastic STED nanoscopy of millisecond dynamics *Nat. Methods* **12** 827–30

[15] Hou S, Lang X and Welsher K 2017 Robust real-time 3D single-particle tracking using a dynamically moving laser spot *Opt. Lett.* **42** 2390

[16] Korpel A 1997 *Acousto-Optics* (New York: Marcel Dekker, Inc)

[17] Klein W R and Cook B D 1967 Unified approach to ultrasonic light diffraction *IEEE Trans. Sonics Ultrason.* **14** 123–34

[18] Raman C V and Nagendra Nath N S 1935 The diffraction of light by high frequency sound waves: part I *Proc. Indian Acad. Sci.* A **2** 406–12

[19] Surdo S and Duocastella M 2019 Fast acoustic light sculpting for on-demand maskless lithography *Adv. Sci.* **6** 1900304

[20] Dixon R W 1967 Acoustic diffraction of light in anisotropic media *IEEE J. Quantum Electron.* **3** 85–93

[21] Goutzoulis A P and Pape D R *Design and Fabrication of Acousto-Optic Devices* (New York: Marcel Dekker, Inc) 1994

[22] Lechleiter J D, Lin D T and Sieneart U 2002 Multi-photon laser scanning microscopy using an acoustic optical deflector *Biophys. J.* **83** 2292–9

[23] Harris S E and Wallace R W 1969 Acousto-optic tunable filter *J. Opt. Soc. Am.* **59** 744–7

[24] Suhre D R 1992 Spatial resolution of imaging noncollinear acousto-optic tunable filters *Opt. Eng.* **31** 2118

[25] Wachman E S, Niu W H and Farkas D L 1997 AOTF microscope for imaging with increased speed and spectral versatility *Biophys. J.* **73** 1215–22

[26] Zunino A, Surdo S and Duocastella M 2019 Dynamic multifocus laser writing with acousto-optofluidics *Adv. Mater. Technol.* **4** 1–7

[27] Gliko O, Brownell W E and Saggau P 2009 Fast two-dimensional standing-wave total-internal-reflection fluorescence microscopy using acousto-optic deflectors *Opt. Lett.* **34** 836–8

[28] Olivier N, Mermillod-Blondin A, Arnold C B and Beaurepaire E 2009 Two-photon microscopy with simultaneous standard and extended depth-of-field using a tunable acoustic gradient-index lens *Opt. Lett.* **34** 1684–6

[29] Mermillod-Blondin A, McLeod E and Arnold C B 2008 High-speed varifocal imaging with a tunable acoustic gradient index of refraction lens *Opt. Lett.* **33** 2146–8

[30] Duocastella M, Sun B and Arnold C B 2012 Simultaneous imaging of multiple focal planes for three-dimensional microscopy using ultra-high-speed adaptive optics *J. Biomed. Opt.* **17** 050505

[31] Piazza S, Bianchini P, Sheppard C, Diaspro A and Duocastella M 2018 Enhanced volumetric imaging in 2-photon microscopy via acoustic lens beam shaping *J. Biophoton.* **11** e201700050

[32] McLeod E, Hopkins A B and Arnold C B 2006 Multiscale Bessel beams generated by a tunable acoustic gradient index of refraction lens *Opt. Lett.* **31** 3155–7

[33] Dean K M and Fiolka R 2014 Uniform and scalable light-sheets generated by extended focusing *Opt. Express* **22** 26141

[34] Duocastella M, Arnold C B and Puchalla J 2017 Selectable light-sheet uniformity using tuned axial scanning *Microsc. Res. Tech.* **80** 250–9

[35] Duocastella M and Arnold C B 2013 Enhanced depth-of-field laser processing using an ultra-high-speed axial scanner *Appl. Phys. Lett.* **102** 061113

[36] Zong W *et al* 2015 Large-field high-resolution two-photon digital scanned light-sheet microscopy *Cell Res.* **25** 254–7

[37] Power R M and Huisken J 2018 Adaptable, illumination patterning light sheet microscopy *Sci. Rep.* **8** 1–11

[38] Kang S, Dotsenko E, Amrhein D, Theriault C and Arnold C B 2018 Ultra-high-speed variable focus optics for novel applications in advanced imaging *Proc. of SPIE—The Int. Society for Optical Engineering* vol 10539

[39] Grulkowski I, Szulzycki K and Wojtkowski M 2014 Microscopic OCT imaging with focus extension by ultrahigh-speed acousto-optic tunable lens and stroboscopic illumination *Opt. Express* **22** 31746

[40] Yang X, Jiang B, Song X, Wei J and Luo Q 2017 Fast axial-scanning photoacoustic microscopy using tunable acoustic gradient lens *Opt. Express* **25** 7349–57

[41] Fahrbach F O, Voigt F F, Schmid B, Helmchen F and Huisken J 2013 Rapid 3D light-sheet microscopy with a tunable lens *Opt. Express* **21** 21010–26

[42] Olarte O E, Andilla J, Artigas D and Loza-Alvarez P 2015 Decoupled illumination detection in light sheet microscopy for fast volumetric imaging *Optica* **2** 702

[43] Tomer R, Lovett-barron M, Kauvar I, Broxton M and Deisseroth K 2015 Resource SPED light sheet microscopy : fast mapping of biological system structure and function *Cell* **163** 1796–806

[44] Duocastella M, Sancataldo G, Saggau P, Ramoino P, Bianchini P and Diaspro A 2017 Fast inertia-free volumetric light-sheet microscope *ACS Photonics* **4** 1797–804

[45] Kong L, Tang J, Little J P, Yu Y, Lämmermann T, Lin C P, Germain R N and Cui M 2015 Continuous volumetric imaging via an optical phase-locked ultrasound lens *Nat. Methods* **12** 759–62

[46] Gavryusev V *et al* 2019 Dual-beam confocal light-sheet microscopy via flexible acousto-optic deflector *J. Biomed. Opt.* **24** 106504

[47] Diaspro A 2013 Taking three-dimensional two-photon excitation microscopy further: encoding the light for decoding the brain *Microsc. Res. Tech.* **76** 985–7

[48] Chen T H, Ault J T, Stone H A and Arnold C B 2017 High-speed axial-scanning wide-field microscopy for volumetric particle tracking velocimetry *Exp. Fluids* **58** 1–7

[49] Szulzycki K, Savaryn V and Grulkowski I 2018 Rapid acousto-optic focus tuning for improvement of imaging performance in confocal microscopy (invited) *Appl. Opt.* **57** C14

[50] Duocastella M, Theriault C and Arnold C B 2016 Three-dimensional particle tracking via tunable color-encoded multiplexing *Opt. Lett.* **41** 863–6

[51] Donnert G, Eggeling C and Hell S W 2007 Major signal increase in fluorescence microscopy through dark-state relaxation *Nat. Methods* **4** 81–86

[52] Duocastella M, Vicidomini G and Diaspro A 2014 Simultaneous multiplane confocal microscopy using acoustic tunable lenses *Opt. Express* **22** 19293

[53] Har-Gil H, Golgher L, Israel S, Kain D, Cheshnovsky O, Parnas M and Blinder P 2018 PySight: plug and play photon counting for fast continuous volumetric intravital microscopy *Optica* **5** 1104

[54] Wei M T, Elbaum-Garfinkle S, Holehouse A S, Chen C C H, Feric M, Arnold C B, Priestley R D, Pappu R V and Brangwynne C P 2017 Phase behaviour of disordered proteins underlying low density and high permeability of liquid organelles *Nat. Chem.* **9** 1118–25

[55] Kong L, Tang J and Cui M 2016 Multicolor multiphoton in vivo imaging flow cytometry *Opt. Express* **24** 6126–35

[56] Kong L, Little J P and Cui M 2016 Motion quantification during multi-photon functional imaging in behaving animals *Biomed. Opt. Express* **7** 3686

[57] Karagyozov D, Mihovilovic Skanata M, Lesar A and Gershow M 2018 Recording neural activity in unrestrained animals with three-dimensional tracking two-photon microscopy *Cell Rep.* **25** 1371–83

[58] Huang C, Tai C Y, Yang K P, Chang W K, Hsu K J, Hsiao C C, Wu S C, Lin Y Y, Chiang A S and Chu S W 2019 All-optical volumetric physiology for connectomics in dense neuronal structures *iScience* **22** 133–46

[59] Martin C, Li T, Hegarty E, Zhao P, Mondal S and Ben-Yakar A 2018 Line excitation array detection fluorescence microscopy at 0.8 million frames per second *Nat. Commun.* **9** 1–10

[60] Chen X, Leischner U, Rochefort N L, Nelken I and Konnerth A 2011 Functional mapping of single spines in cortical neurons in vivo *Nature* **475** 501–5

[61] Bullen A, Patel S S and Saggau P 1997 High-speed, random-access fluorescence microscopy: I. High-resolution optical recording with voltage-sensitive dyes and ion indicators *Biophys. J.* **73** 477–91

[62] Reddy G D and Saggau P 2005 Fast three-dimensional laser scanning scheme using acousto-optic deflectors *J. Biomed. Opt.* **10** 064038

[63] Guessoum A 2019 Scanning velocity measurement of an acousto-optic deflector *Opt. Spectrosc.* **126** 443–9

[64] Liu X, Lv X, Zeng S, Zhou W and Luo Q 2009 Noncontact and nondestructive identification of neural circuits with a femtosecond laser *Appl. Phys. Lett.* **94** 061113

[65] Wang K, Liu Y, Li Y, Guo Y, Song P, Zhang X, Zeng S and Wang Z 2011 Precise spatiotemporal control of optogenetic activation using an acousto-optic device *PloS One* **6** e28468

[66] Xia Y, Zhao Y, Yang M, Zeng S and Shu Y 2014 Regulation of action potential waveforms by axonal GABAa receptors in cortical pyramidal neurons *PloS One* **9** e100968

[67] Bansal V, Patel S and Saggau P 2003 A high-speed confocal laser-scanning microscope based on acousto-optic deflectors and a digital micromirror device *Conf. Proc. IEEE Eng. Med. Biol. Soc.* **3** 2124–7

[68] Hoover E E and Squier J A 2013 Advances in multiphoton microscopy technology *Nat. Photon.* **7** 93–101

[69] Iyer V, Losavio B E and Saggau P 2003 Compensation of spatial and temporal dispersion for acousto-optic multiphoton laser-scanning microscopy *J. Biomed. Opt.* **8** 460

[70] Zeng S, Lv X, Zhan C, Chen W R, Xiong W, Jacques S L and Luo Q 2006 Simultaneous compensation for spatial and temporal dispersion of acousto-optical deflectors for two-dimensional scanning with a single prism *Opt. Lett.* **31** 1091

[71] Lv X, Zhan C, Zeng S, Chen W R and Luo Q 2006 Construction of multiphoton laser scanning microscope based on dual-axis acousto-optic deflector *Rev. Sci. Instrum.* **77** 046101

[72] Grewe B F, Langer D, Kasper H, Kampa B M and Helmchen F 2010 High-speed in vivo calcium imaging reveals neuronal network activity with near-millisecond precision *Nat. Methods* **7** 399–405

[73] Otsu Y, Bormuth V, Wong J, Mathieu B, Dugué G P, Feltz A and Dieudonné S 2008 Optical monitoring of neuronal activity at high frame rate with a digital random-access multiphoton (RAMP) microscope *J. Neurosci. Methods* **173** 259–70

[74] Iyer V, Hoogland T M and Saggau P 2006 Fast functional imaging of single neurons using random-access multiphoton (RAMP) microscopy *J. Neurophysiol.* **95** 535–45

[75] Losavio B E, Iyer V and Saggau P 2009 Two-photon microscope for multisite microphotolysis of caged neurotransmitters in acute brain slices *J. Biomed. Opt.* **14** 064033

[76] Salomé R, Kremer Y, Dieudonné S, Léger J F, Krichevsky O, Wyart C, Chatenay D and Bourdieu L 2006 Ultrafast random-access scanning in two-photon microscopy using acousto-optic deflectors *J. Neurosci. Methods* **154** 161–74

[77] Liu X, Quan T, Zeng S and Lv X 2011 Identification of the direction of the neural network activation with a cellular resolution by fast two-photon imaging *J. Biomed. Opt.* **16** 080506

[78] Duemani Reddy G, Kelleher K, Fink R and Saggau P 2008 Three-dimensional random access multiphoton microscopy for functional imaging of neuronal activity *Nat. Neurosci.* **11** 713–20

[79] Vučinić D and Sejnowski T J 2007 A compact multiphoton 3D imaging system for recording fast neuronal activity *PloS One* **2** e699

[80] Konstantinou G, Kirkby P A, Evans G J, Naga Srinivas Nadella K M, Griffiths V A, Mitchell J E and Angus Silver R 2016 Dynamic wavefront shaping with an acousto-optic lens for laser scanning microscopy *Opt. Express* **24** 6283

[81] Akemann W, Léger J-F, Ventalon C, Mathieu B, Dieudonné S and Bourdieu L 2015 Fast spatial beam shaping by acousto-optic diffraction for 3D non-linear microscopy *Opt. Express* **23** 28191

[82] Bechtold P, Hohenstein R and Schmidt M 2013 Beam shaping and high-speed, cylinder-lens-free beam guiding using acousto-optical deflectors without additional compensation optics *Opt. Express* **21** 14627–35

[83] Katona G, Szalay G, Maák P, Kaszás A, Veress M, Hillier D, Chiovini B, Vizi E S, Roska B and Rózsa B 2012 Fast two-photon in vivo imaging with three-dimensional random-access scanning in large tissue volumes *Nat. Methods* **9** 201–8

[84] Szalay G *et al* 2016 Fast 3D imaging of spine, dendritic, and neuronal assemblies in behaving animals *Neuron* **92** 723–38

[85] Fernández-Alfonso T, Nadella K M N S, Iacaruso M F, Pichler B, Roš H, Kirkby P A and Silver R A 2014 Monitoring synaptic and neuronal activity in 3D with synthetic and genetic indicators using a compact acousto-optic lens two-photon microscope *J. Neurosci. Methods* **222** 69–81

[86] Chamberland S *et al* 2017 Fast two-photon imaging of subcellular voltage dynamics in neuronal tissue with genetically encoded indicators *Elife* **6** 1–35

[87] Jiang R, Zhou Z, Lv X and Zeng S 2012 Wide-band acousto-optic deflectors for large field of view two-photon microscope *Rev. Sci. Instrum.* **83** 043709

[88] Nadella K M N S, Roš H, Baragli C, Griffiths V A, Konstantinou G, Koimtzis T, Evans G J, Kirkby P A and Silver R A 2016 Random-access scanning microscopy for 3D imaging in awake behaving animals *Nat. Methods* **13** 1001–4

[89] Saggau P 2006 New methods and uses for fast optical scanning *Curr. Opin. Neurobiol.* **16** 543–50

[90] Wu Y, Wu X, Toro L and Stefani E 2015 Resonant-scanning dual-color STED microscopy with ultrafast photon counting: a concise guide *Methods* **88** 48–56

[91] Chen Z, Mc Larney B, Rebling J, Deán-Ben X L, Zhou Q, Gottschalk S and Razansky D 2020 High-speed large-field multifocal illumination fluorescence microscopy *Laser Photonics Rev.* **14** 1900070

[92] Chong E Z, Panniello M, Barreiros I, Kohl M M and Booth M J 2019 Quasi-simultaneous multiplane calcium imaging of neuronal circuits *Biomed. Opt. Express* **10** 267–92

[93] Diebold E D, Buckley B W, Gossett D R and Jalali B 2013 Digitally synthesized beat frequency multiplexing for sub-millisecond fluorescence microscopy *Nat. Photon.* **7** 806–10

[94] Mikami H *et al* 2018 Ultrafast confocal fluorescence microscopy beyond the fluorescence lifetime limit *Optica* **5** 117–26

[95] Tsyboulski D, Orlova N, Ledochowitsch P and Saggau P 2019 Two-photon frequency division multiplexing for functional in vivo imaging: a feasibility study *Opt. Express* **27** 4488–503

[96] Tsyboulski D, Orlova N and Saggau P 2017 Amplitude modulation of femtosecond laser pulses in the megahertz range for frequency-multiplexed two-photon imaging *Opt. Express* **25** 9435–42

[97] Buckley B W, Akbari N, Diebold E D, Adam J and Jalali B 2015 Radiofrequency encoded angular-resolved light scattering *Appl. Phys. Lett.* **106** 123701

[98] Liao C S, Wang P, Huang C Y, Lin P, Eakins G, Bentley R T, Liang R and Cheng J X 2018 In vivo and in situ spectroscopic imaging by a handheld stimulated Raman scattering microscope *ACS Photonics* **5** 947–54

[99] Wei X, Shen Y, Jing J C, Hemphill A S, Yang C, Xu S, Yang Z and Wang L V 2020 Real-time frequency-encoded spatiotemporal focusing through scattering media using a programmable 2D ultrafine optical frequency comb *Sci. Adv.* **6** 1–9

[100] Gómez-García P A, Garbacik E T, Otterstrom J J, Garcia-Parajo M F and Lakadamyali M 2018 Excitation-multiplexed multicolor superresolution imaging with fm-STORM and fm-DNA-PAINT *Proc. Natl Acad. Sci. USA* **115** 12991–6

[101] Ren Y, Wu J, Lai Q T K, Lai H M, Siu D M D, Wu W, Wong K K Y and Tsia K K 2020 Parallelized volumetric fluorescence microscopy with a reconfigurable coded incoherent light-sheet array *Light Sci. Appl.* **9** 8

[102] Garbacik E T, Sanz-Paz M, Borgman K J E, Campelo F and Garcia-Parajo M F 2018 Frequency-encoded multicolor fluorescence imaging with single-photon-counting color-blind detection *Biophys. J.* **115** 725–36

[103] Mandracchia B, Hua X, Guo C, Son J, Urner T and Jia S 2020 Fast and accurate sCMOS noise correction for fluorescence microscopy *Nat. Commun.* **11** 1–12

[104] Palubiak D P and Deen M J 2014 CMOS SPADs: design issues and research challenges for detectors, circuits, and arrays *IEEE J. Sel. Top. Quantum Electron.* **20** 6000718

[105] Barbastathis G, Ozcan A and Situ G 2019 On the use of deep learning for computational imaging *Optica* **6** 921

[106] Deneux T, Kaszas A, Szalay G, Katona G, Lakner T, Grinvald A, Rozsa B and Vanzetta I 2016 Accurate spike estimation from noisy calcium signals for ultrafast three-dimensional imaging of large neuronal populations in vivo *Nat. Commun.* **7** 12190

[107] Sakaki K D R, Coleman P, Toth T D, Guerrier C and Haas K 2018 Automating event-detection of brain neuron synaptic activity and action potential firing in vivo using a random-access multiphoton laser scanning microscope for real-time analysis *Proc. Annu. Int. Conf. IEEE Eng. Med. Biol. Soc. EMBS* (*July 2018*) pp 3017–23

[108] Bianchini P, Saggau P and Diaspro A 2020 An inertia-free beam scanning device for single-wavelength 2PE-STED nanoscopy *J. Phys. D: Appl. Phys.* **53** 324001